Leaves in iron oxide : remarkable preservation of a neogene flora from New Caledonia

Emma R Locatelli, Derek E.G. Briggs, Andrew Leslie, Jérôme Munzinger, Philippe Grandcolas, Porter P. Lowry, David J. Cantrill, Pierre Maurizot, Dominique Cluzel, Nicolas Folcher, et al.

LEAVES IN IRON OXIDE: REMARKABLE PRESERVATION OF A NEOGENE FLORA FROM NEW CALEDONIA

EMMA R. LOCATELLI[1], DEREK E.G. BRIGGS[1,2], ANDREW LESLIE[3], JÉRÔME MUNZINGER[4], PHILIPPE GRANDCOLAS[5], PORTER P. LOWRY II[5,6], DAVID J. CANTRILL[7], PIERRE MAURIZOT[8], DOMINIQUE CLUZEL[9], NICOLAS FOLCHER[9], ROMAIN GARROUSTE[5] AND ANDRÉ NEL[5]

[1]*Department of Earth and Planetary Sciences, Yale University, New Haven, Connecticut, 06520, USA, emma.locatelli@yale.edu*

[2]*Yale Peabody Museum of Natural History, New Haven, Connecticut, 06520, USA, derek.briggs@yale.edu*

[3]*Department of Geological Sciences, Stanford University, 450 Jane Stanford Way, Stanford CA 94305, USA, aleslieb@stanford.edu*

[4]*AMAP Université Montpellier, IRD, CIRAD, CNRS, INRAE, F-34000 Montpellier, France, jerome.munzinger@ird.fr*

[5]*Institut de Systématique, Évolution, Biodiversité (ISYEB), Muséum national d'Histoire naturelle, CNRS, Sorbonne Université, EPHE, Université des Antilles, CP50, 57 rue Cuvier 75005 Paris, France, pg@mnhn.fr, anel@mnhn.fr, romain.garrouste@mnhn.fr*

[6]*Missouri Botanical Garden, 4344 Shaw Boulevard, St. Louis, Missouri, 63110, USA, pete.lowry@mobot.org*

[7]*Royal Botanic Gardens Victoria, Melbourne, South Yarra, Victoria, 3004, Australia, David.Cantrill@rbg.vic.gov.au*

[8]*Service Géologique de la Nouvelle-Calédonie, 1 ter rue Unger, BP M@, 98849, Nouméa Cédex, New Caledonia*

pierre.maurizot@gouv.nc

[9] *University of New Caledonia, ISEA-EA 7484, BP R4, 98 851 Nouméa, New Caledonia*

dominique.cluzel@unc.nc, *folchernicolas@gmail.com*

Keywords: paleobotany, taphonomy, New Caledonia, exceptional preservation, tropics

ABSTRACT: A Neogene hematite-goethite concretionary 'ironstone' horizon in lateritized fluvial sediments in the Massif du Sud of New Caledonia yields abundant fossil dicotyledonous angiosperm leaves. The leaves are preserved in iron oxide, mainly goethite, which replicates the morphology and anatomy of the leaf tissues and comprises 73% of the matrix. Organic remains are minimal and associated with aluminosilicate clay. Leaf tissues are preserved three-dimensionally in multiple ways including casts/molds, permineralization/petrifaction, and replacement. Although the mesophyll is less well preserved, reflecting its greater susceptibility to decay, cellular details of vascular and epidermal tissues are commonly evident. Analyses of leaves from an analogous modern setting reveal the early encrustation and impregnation of tissues by amorphous iron-oxides and clays in association with a microbial biofilm. We propose a taphonomic model in which the fossil leaves, like their modern counterparts, were permeated by iron oxides due to the high availability of iron derived from weathering of ultramafic basement. In contrast to the iron-rich aluminosilicate coatings that form in relatively iron-poor settings, the unusually high concentration of dissolved iron oxides permitted rapid anatomical preservation.

INTRODUCTION

A role for iron in the preservation of leaf impressions in the fossil record has long been recognized (Krystofovich 1944; Spicer 1977). Such impression fossils provide a window into ancient vegetation in sediments deposited in oxidizing conditions (e.g., upper units of the Clarkia lagerstätte, Idaho, USA: Smiley et al. 1975). However, despite the high fidelity preservation of surface details in some cases (e.g., Dakota Sandstone: Retallack and Dilcher 2012), anatomy rarely survives and these iron-coated leaves provide limited morphological information (Crane and Dilcher 1984). In contrast, permineralized leaves – those in which tissues have been impregnated by minerals and are preserved in three-dimensions – retain more biological information (Schopf 1975; Spicer 1989; Locatelli 2014). The most common minerals involved in this type of preservation are silica (e.g., the Devonian Rhynie Chert), calcium carbonate (e.g., coal balls, travertines), and pyrite (e.g., the Eocene London Clay) (Locatelli 2014). Where iron oxides preserve plant fossils in three dimensions (e.g., Mohr and Friis 2000) this is usually the result of *in situ* weathering of original pyrite. Primary permineralization in iron oxide has been reported from the Permian Clear Fork Group red beds in Texas (Chaney et al. 2009), although most of the leaves are preserved as organic compressions, and from Miocene channel iron deposits in the Pilbara region of Western Australia (Morris and Ramanaidou 2007; Ramanaidou and Morris 2010). More recently a diverse biota from the Miocene McGraths Flat in New South Wales has been described with cellular details preserved in iron oxides (McCurry et al. 2022). Here we describe the taphonomy of an exceptionally preserved fossil flora from New Caledonia which includes angiosperm leaves, seeds and flowers, gymnosperm leaves, with rare associated insects, in Neogene fluvial and lacustrine deposits developed on ultramafic basement (Bourdon

and Podwojewski 1988; Locatelli 2013; Garrouste et al. 2021). The leaves preserve cellular detail in three-dimensions in primary iron oxides precipitated externally, at least initially, on a microbially mediated iron-rich clay template. We compare these results to analyses of modern leaves collected in an iron-rich stream in New Caledonia and offer a taphonomic model for this unusual form of fossilization. Microbial biofilms and authigenic mineralization play a role in the preservation of leaves, even in very iron rich settings.

GEOLOGICAL SETTING

The main island of New Caledonia, the Grande Terre, consists of a Gondwanan basement that separated from the eastern margin of Australia in the Late Cretaceous (Hayes and Ringis 1973; Uruski and Wood 1991; Gaina et al. 1998; Eissen et al. 1998; Chevillotte et al. 2006; Maurizot and Vendé-Leclerc 2009; Yang et al. 2013). After the split from Gondwana, the island underwent a complex series of tectonic events, most notably the obduction of an ultramafic ophiolite sequence during the late Eocene (38–34 Ma) now subdivided by tectonics and erosion into several units of which the Massif du Sud, in the south of New Caledonia, is the largest (Pelletier 2006; Maurizot and Collot 2009; Maurizot and Campbell 2020). The tectonic chronology is summarized in a number of publications (Crawford et al. 2003; Sdrolias 2003; Cluzel et al. 2012; Maurizot and Collot 2009; Maurizot and Mortimer 2020).

Following obduction, a first episode of extensive lateritization (Herbillon and Nahon 1988) of the ultramafic rocks developed a thick regolith topped by ferricrete. Tropical weathering of the ultramafic ophiolite probably occurred as soon as the early Oligocene and continued after the early Miocene, as evidenced by a series of ferricrete-capped terraces and paleolaterites within

62 early Miocene deposits (Chevillote et al. 2006; Sevin et al. 2011). Early Miocene uplift resulted
63 in regolith erosion, the products of which accumulated in small intermontane basins, which were
64 in turn subject to weathering and the formation of a new ferricrete cap. New Caledonia has been
65 moving northward within the tropical belt since the Miocene (Sdrolias et al. 2003) and terrestrial
66 temperatures have remained relatively constant (within 2°C) for the last 6 million years (Tardy
67 and Roquin 1998). The present geological landscape of the Massif du Sud (Folcher et al. 2015) is
68 a result of erosion. Laterization of the peridotite results in the leaching of Si and Mg downward,
69 concentrating Fe, Ni, and Co in the upper layers of oxisol, the ferricrete cap, and underlying red
70 limonite (Yang et al. 2013): Fe comprises up to 40% by weight of these layers, primarily in the
71 form of goethite (Chevillote et al. 2006). The erosion and transport of the soils and ferricrete cap
72 resulted in the accumulation of goethite-dominated sediments in fluvio-lacustrine deposits, both
73 as transported grains and authigenic minerals (Sevin et al. 2012). Within the fluvio-lacustrine
74 sediments, and later within the soils, concretionary ironstone horizons (duricrusts) formed in situ
75 with the precipitation of hematite and goethite cements around existing grains, filling voids and
76 greatly reducing the porosity and permeability of the horizon (Sevin et al. 2011; Folcher et al.
77 2015). Duricrusts commonly contain root casts and trunks preserved in growth position (Folcher
78 et al. 2015; Sevin et al. 2020).
79 Neogene (post 25 Ma) fluvio-lacustrine deposits (Guillon et al. 1972; Maurizot and Collot
80 2009) are distributed across the surface of the southernmost portion of the Grande Terre (Fig. 1).
81 Many of these deposits are concealed beneath the recent regolith, but several have been eroded
82 and provide good exposure (Folcher et al. 2015). The timing of their deposition is unknown, as
83 the iron-oxide dominated sediments are not suitable for radiogenic dating, lack index fossils, and

paleomagnetic dating techniques reveal ages ranging from latest Oligocene to Holocene (Sevin et al. 2012; Folcher et al. 2015; Maurizot et al. 2020; Sevin et al. 2020).

MATERIALS AND METHODS

Fossil Leaves

Samples of fossil dicotyledonous angiosperm leaves (Fig. 2) were collected from a ~2 cm thick duricrust of ferruginous silt and claystone within uplifted fluvio-lacustrine deposits in the Rivière des Lacs Basin (Garrouste et al. 2021, Supplementary Figure 7) toward the southern end of the Massif du Sud (Fig. 1). The roadside exposure is along the Route de Carénage, approximately 200 m north of the entrance to the Chutes de la Madeleine Natural Reserve (-22.229°, 166.851°) (Fig. 1). Abundant dicotyledonous angiosperm leaves dominate the flora, which also includes flowers, seeds, and wood (Garrouste et al. 2021). The samples are the property of the government of New Caledonia, Service Géologique de la Nouvelle-Calédonie (SGNC) and are held by the Direction de l'Industrie, des mines et de l'énergie de la Nouvelle-Calédonie (DIMENC).

Modern Leaves

Leaves from a small stream south of Les Chutes de Madeleine (-22.273°, 166.931°) were collected for investigation as a modern analog because conditions in this stream are likely similar to those in the fluvial system in which the fossils were deposited. The vegetation surrounding the stream is composed primarily of shrubs adapted to the acidic nature of the iron-rich, clay-poor oxisols that occur in the study area (Jaffré 1992; Isnard et al. 2016).

The stream was at low, dry-season levels at the time of collection (April 2013), as indicated by terraces on the stream banks and the accumulation of leaves and other debris higher on the bank. Fifteen leaves were collected from the bottom of a shallow pool in the stream, and fifteen from within the top layer of sediment on the stream bank; total sediment thickness was not measured. The ages of the two sample sets are unknown, and they may represent multiple wet/dry seasons. The leaves were dried slowly by placing them in absorbent paper in a temperature-controlled room to retain their integrity and prevent any significant further decay.

Microscopy and EDS and XRD Analysis

A total of 40 dicotyledonous angiosperm leaf fossils were examined using light microscopy (Fig. 2). Morphological and anatomical preservation of both the fossil and modern leaves were investigated using scanning electron microscopy (SEM) (Figs 3, 5–8) and elemental composition was analyzed using electron-dispersive-X-ray spectroscopy (EDS) (Figs 3, 8).

Material for SEM was obtained from the margins of fossil leaves by extracting small portions of leaf and matrix with a scalpel; 25 such fragments were sampled. Three polished thin sections were made for elemental and mineralogical analysis. Six modern leaves, three from the stream bed and three from the bank sediment, were sampled for SEM analysis. Samples were mounted on aluminum stubs, platinum coated using a Cressington 108 Auto Sputter Coater and examined using a FEI XL-30 field emission gun environmental SEM equipped with an EDAX energy dispersive X-ray spectrometer. Point spectra were taken from different tissues at an accelerating voltage of 10 kV and collection time of 100 seconds.

Material for X-ray diffraction analysis was scraped from the surface of modern leaves with a scalpel. The powder sample was analyzed with a bench-top MiniFlex 600 (Rigaku) which uses

Cu radiation and a wide area scintillation counter detection system. It was operated at 600W (40kV – 15mA) to collect data in reflection mode with a 2θ scan range of 3° to 90° at 5°/minute and a step size of 0.02°. The data were analyzed using Rigaku Data Analysis Software (PDXL 2).

Raman Spectroscopy

Four standard 30 μm thick petrographic thin sections were cut and polished to create vertical sections through the fossil leaf-bearing concretionary layer and transverse sections through the leaves themselves. Raman spectra were obtained using a Horiba Jobin Yvon Labram HR800 spectrometer equipped with a 532 nm laser with a hole size of 300 μm, a slit size of 100 μm, and a grating of 1800 grooves/mm. Spectra were acquired for 6 seconds with 10 repetitions. A neutral density filter was used to reduce the laser power as iron oxides other than hematite are prone to burning, which results in shifting and transformation of the spectrum (Hanesch 2009). A total of 30 grains, 5 each from 3 different fossil leaves and 5 each from the matrix associated with the 3 different leaves, were analyzed for each thin section. At low magnification, the darker red matrix and orange to yellow leaves are markedly distinct. Leaf and matrix areas were identified, and grains within those regions were selected at random, providing they were large enough to sample (> 2 μm diameter).

RESULTS

Fossil Leaves

Composition.—EDS maps and point spectra on the thin sections show that the fossil leaves are composed predominantly of a mixture of iron oxides and aluminosilicate clays (Fig. 3). Residual carbonaceous material, revealed by backscatter electron imaging as dark areas within the leaf and by elemental mapping (Fig. 3B, 3C), is restricted to discrete particles encased in a very fine-grained iron-rich clay (Fig. 3B, 3C). The rest of the leaf tissue is composed of iron oxide, with small amounts of carbon, aluminum and silicon (Fig. 3C, Supplement). The matrix is composed of carbon-, aluminum- and silicon-poor iron oxides, which are enriched in chromium (Fig. 3C, supplement).

Raman spectroscopy identified 4 of the 15 matrix grains (27%) as hematite (Fe_2O_3), evidenced by diagnostic peaks at 225, 300, and 1321 cm^{-1} and a weaker peak at 412 (Hanesch 2009) (Fig. 4A). The majority of the grains (11, i.e., 73%) were goethite (α-FeOOH), evidenced by diagnostic peaks at 385 and weaker ones at 225, 299, 548, and 681 cm^{-1} (Hanesch 2009) (Fig. 4B). The predominantly fine-grained isodimensional crystalline nature of the matrix with acicular outgrowths is also consistent with a mixture of hematite and goethite (Schwertmann and Latham 1986; Cornell et al. 1989) (Fig. 5A).

All 15 grains sampled from the fossil leaves were identified as goethite (Fig. 4C). Figure 4C shows a spectrum characteristic of 12 of the 15 leaf grains sampled; the other 3 leaf grains lacked the definitive peak at 385 cm^{-1} but yielded a wide peak at 400 cm^{-1} (not figured). This is consistent with other natural samples of goethite ('yellow ochre') and reflects merging of the 385 cm^{-1} peak with a small one at 417 cm^{-1} (Hanesch 2009), a slight shift attributed to different crystallinities of the mineral which was confirmed by SEM analysis. SEM of the leaf tissues revealed mineral forms ranging from acicular crystals and crystal bundles to a nanogranular and amorphous texture. Acicular crystals and crystal bundles range in length from 100 nm to 2 μm,

consistent with the acicular form of goethite crystals that precipitate in void spaces in a silica and aluminum-poor medium (Fig. 5B, 5C) (Fordham et al. 1984; Cornell 1985; Cornell et al. 1987; Schwertmann 1988). The well-defined goethite crystals are found in voids, such as cell lumina, whereas minerals that appear nanogranular to amorphous form a mesh-like fabric comprised of individual crystals on the order of a few tens of nm in length and width (Fig. 5D), which we interpret as very fine-grained iron-rich aluminosilicate clays and iron oxides that were too small to analyze individually using Raman spectroscopy, but for which EDS revealed a composition of predominantly iron, aluminum, silicon, and oxygen. It is this nanogranular to amorphous material that is involved in the fine preservation of both internal (e.g., epidermal cells, veins, stomata) and external (e.g., leaf gland) anatomy.

Anatomical and Morphological Preservation.—SEM of fossil leaf tissues revealed that they are preserved in multiple ways including permineralization/petrifaction (a gradation from retention of organic cell walls to loss and replacement of all carbonaceous remains of the cuticle), replacement, and as casts or molds in iron oxides; individual leaves often exhibit several modes of preservation. The three-dimensionality of the preservation was confirmed by SEM including backscatter electron microscopy (Fig. 6A, 6B).

Vascular tissues are usually preserved as hollow tubes with the walls preserved either as a cast or via replacement (Fig. 6C), or as solid bundles, which are likely internal casts (Fig. 6D). Where vascular tissues are preserved as hollow tubes mineral grain size varies, which may indicate precipitation at different rates and times, and boundaries between cells are rarely discernable. Internal casts may preserve individual cells of the vessel lumen (Fig. 6D). In several samples, vascular tissues exhibit evidence of decay followed by replacement: in these cases, the

197 cellulose-dominated cell wall has decayed leaving lignified secondary cell wall thickenings that
198 were subsequently replaced by iron oxides (Fig. 6E).

199 Mesophyll is the least well preserved of the leaf tissues. Only poor cellular preservation was
200 observed in the thin sections (Fig. 6A), although the overarching structure of some leaves is
201 discernible. Visibility of preserved tissues under the SEM depends on fortuitous fractures in the
202 fossil material: the matrix is cemented so thoroughly that it cannot be removed using needles or
203 other tools. Typically, the mesophyll of leaves has decayed away leaving spaces infilled by iron
204 oxides with no orientation or pattern (Fig. 6J).

205 Epidermal details, including cells, stomata, and glands, are preserved predominantly as
206 molds and casts and via replacement. Stomata were most commonly evident from the interior of
207 the leaf (Fig. 6F). The guard cells of the stomata are preserved as external molds, and the walls
208 of cells surrounding the stomata have been replaced (Fig. 6G). Some epidermal cell walls are
209 preserved as residual cuticle, whereas others have been replaced by iron oxides (Fig. 6H). When
210 cells are preserved as internal casts, coarser mineral grains on the order of several microns mask
211 finer details (Fig. 6I). The walls of epidermal cells can also be replaced by iron oxides, revealed
212 when fractures through the leaf tissue are parallel with the leaf surface (Fig. 6F). Where external
213 epidermal features are preserved via replacement by iron oxides at a cellular level, the
214 distribution and morphology of glands across the leaf surface are evident (Fig. 6K, 6L). No
215 trichomes or trichome bases were observed.

216 There was evidence of microbial biofilms (Pacton et al. 2007) on the surface of some leaves,
217 including a diatom (Fig. 7A) and strands and veils of mineralized extracellular polymeric
218 substances (EPS) (Fig. 7B–D).

219

Modern Leaves

Modern leaves collected from stream and bank sediments showed no differences in extent of decay or early diagenesis. Leaves from both settings exhibited a spectrum of decay, damage, and mineralization, from entirely whole with a crust of iron oxides, to partially skeletonized, to almost entirely skeletonized (Fig. 8A). All leaves were covered in a fine layer of iron oxide, up to 0.5 mm thick on some. EDS spectra of the mineral coating revealed an iron-oxide (Fig. 8B), but those closest to the leaf surface contained significantly more aluminum and silicon than the exterior portion of the coating, indicating the presence of aluminosilicate clays in addition to iron oxides (Fig. 8C). The leaves retained significant organic material, but EDS analysis (Fig. 8B) showed that all portions of the leaf were encrusted or impregnated with iron oxides. XRD data showed this material to be predominantly goethite.

A transverse section through a leaf sampled for SEM revealed extensive impregnation of the leaf by iron oxides with highest concentrations on the more porous abaxial side (Fig. 8D, 9). The surface of all of the leaves was covered in a poorly crystalline crust and diatom biofilm (Fig. 8A and 8E). The iron oxide crust was similar in thickness across the leaf, although it was discontinuous in places (Fig. 8F). This discontinuity may be an effect of drying and transport after collection. The crust appeared to have precipitated between layers of EPS (Fig. 8E). The appearance of the crust and composition of the leaves (Supplementary figure) is consistent with ferrihydrite (Loeppert and Clarke 1984), a hydrated ferric oxyhydroxide, which previous taphonomic experiments have shown to form on decaying leaves (Dunn et al. 1997). A portion of skeletonized leaf revealed the infilling of void spaces, impregnation of veins, and coating of cell surfaces by iron oxides (Fig. 8G). Two diatom species were found on all leaves sampled (Fig. 8H, 8I).

DISCUSSION

Mode of Preservation

Fossil leaves and other plant organs with a coating of iron rich-clays have been reported from strata ranging from Silurian to Recent in age, and the process involved has been investigated via taphonomic experiments and the analysis of fossils (Locatelli 2014). Experiments have shown that the microbial biofilms that form during decay attract metal ions, particularly iron and aluminum (Konhauser and Urrutia 1999). Within days to weeks, iron-rich aluminosilicate clays nucleate and precipitate within the EPS matrix (Konhauser et al. 1998; Locatelli et al. 2017). Clay coatings increase the preservation potential of leaves as they slow the rate of microbial decay and increase the integrity of the leaf over longer timescales, allowing further mineralization or lithification (Dunn et al. 1997; Locatelli 2014). The precipitation of a clay and metal oxide coating normally results only in the preservation of the external leaf surfaces in impressions or the protection of organic tissues within compressions rather than the precipitation of minerals within the leaf as in the New Caledonian fossils.

Plant fossil assemblages in which internal tissues are preserved in iron oxides may be the result of in situ weathering of original pyrite, as in the Cretaceous Crato flora from Brazil (Mohr and Friis 2000; Martill et al. 2007). The Permian Clear Fork Group flora from Texas (Mamay 1989; Chaney and DiMichele 2007; Chaney et al. 2009) is a product of direct precipitation of iron oxides. The preservation of the New Caledonian plant fossils appears directly attributable to the unusually high amount of available iron oxides and the rapid formation of duricrust in the weathering profile of the ultramafic basement. In this respect the depositional setting in New Caledonia, both now and in the past, is unusual. The lateritization

of ultramafic rocks results in oxisols with a layered profile, the upper layers of which are dominated by iron oxides but are very poor in silicon and aluminum (0.5–1.7%) (Schwertmann and Latham 1986, Fandeur et al. 2009). Analyses of the red limonite sediments (the layer in which ironstone horizons form) on the Koniambo Massif in northern New Caledonia, for example, revealed a composition of 40–75% iron by weight (Yang et al. 2013). Hematite and goethite are the most common minerals in the red limonite and form *in situ* from the weathering products of the underlying peridotite (Sevin et al. 2012). Goethite is the only iron oxide found in oxisols of higher altitude regions (Schwertmann and Latham 1986). In low altitude regions, such as the area of our study, hematite contributes up to 40% of the modern sediments (Schwertmann and Latham 1986), consistent with the results of the Raman analyses of the matrix in which our fossils are preserved. Similar processes preserve plants and insects where schwertmannite and goethite precipitate on their surfaces in the acid drainage from iron sulfide ores in the Rio Tinto system north of Huelva in south-west Spain (Sánchez España et al. 2007; Fernández-Remolar and Knoll 2008). Here, as in New Caledonia, the precipitates forming in the river today are the same as those in the river terrace which, in Spain, are up to 2 million years old. The spectacular fossils at McGraths Flat in New South Wales are likewise preserved in goethite with local basalts as the source of iron (McCurry et al. 2022). Travertines may also include bands of goethite, ferrihydrite and other oxides (Arana et al. 1979) and in some cases these preserve plants and insects (Nel and Blot 1990; Kanellopoulos et al. 2019).

Ferrihydrite, Goethite, and Hematite

Hydrated iron oxyhydroxide ferrihydrite, which is the first iron oxide adsorbed onto leaves during decay (Dunn et al. 1997), is unstable and quickly undergoes transformation,

289 usually to hematite or goethite, which are the most thermodynamically stable species under
290 oxic conditions, such as those that prevail in the oxisols of New Caledonia (Cornell 1985;
291 Cornell and Giovanoli 1985; Cornell et al. 1987; Cornell and Schwertmann 2006; Fandeur et
292 al. 2009). The transformation of ferrihydrite to either goethite or hematite is controlled by
293 numerous factors, including the amount and type of free sugars, aluminum replacement of
294 iron (III), and water availability (Cornell and Schwertmann 2006 and references therein).
295 Generally, the conditions that favor the transformation of ferrihydrite to goethite (pH 2–5, 9–
296 12; <30°C) greatly inhibit the transformation to hematite and *vice versa* (Schwertmann et al.
297 2004; Cornell and Schwertmann 2006). Aluminum-replacement of iron in the ferrihydrite
298 matrix can prevent its transformation to goethite (Fritsch et al. 2002).
299 Surface waters and soils from the region where the fossils occur (lowlands; mean annual
300 temperature 23–24°C) are generally acidic with a pH of 4.4–5 (Enright et al. 2001; Read et al.
301 2006). Surface temperatures and pH values within this range favor the transformation of
302 ferrihydrite into goethite on multi-year to decadal timescales (Schwertmann et al. 2004;
303 Cudennec and Lecerf 2006). The preservation of leaves in goethite and its dominance in the
304 surrounding matrix indicate that the pH range was relatively constant. The proportion of
305 matrix consisting of hematite (27%) may reflect a transported fraction or dehydration of the
306 matrix ferrihydrite following fossilization (Schwertmann et al. 2004). Thus the near-total
307 replacement of tissues in the New Caledonian fossil flora by iron oxides suggests preservation
308 within a time window of several years to a few decades. However, the rate of decay and
309 mineral precipitation may have varied during alternating water-logged and well-drained or
310 drying conditions (Spicer 1991; Locatelli 2014). During arid phases the reduction or absence
311 of abundant pore waters may have reduced both the rate of decay and mineral precipitation.

312 The modern leaves collected from the stream displayed a range of decay states, but the
313 length of time any individual leaf was in the stream is unknown. There was no evidence of
314 crystalline hematite or goethite on these leaves: the amorphous or nano-granular texture of the
315 mineral crust indicates recent authigenic precipitation. The leaves collected from sediments in
316 the stream bank were also encrusted in a similar aluminum-enriched iron oxide.
317
318 **CONCLUSION**
319
320 Accumulation of the erosion products of laterite profiles developed on ultramafic rocks in
321 the Rivière des Lacs Basin in the southern Massif du Sud of New Caledonia has resulted in
322 surface sediments depleted in aluminum and silicon but greatly enriched in highly mobile iron
323 (III) (Read et al. 2006). As observed in the modern fluvial analogue, accumulation of leaves in
324 low-energy pools within a stream resulted in enhanced fossilization potential. Analyses of
325 fossil leaves and modern analogues suggest that microbes, including diatoms and most likely
326 bacteria, colonized the leaf surface as well as other exposed leaf tissues. Associated
327 extracellular polymeric substances (EPS) resulted in biofilms (Fig. 7) on to which dissolved
328 iron, aluminum, and silicon were adsorbed, resulting in the initial microbially-mediated
329 precipitation of iron- and aluminum oxides and aluminosilicate clay minerals (Konhauser
330 1998) (Figs 7, 8). Elemental analyses reveal that these precipitates on both fossil and modern
331 specimens are iron-rich and silicon-poor (Figs 3, 8, Supplement), consistent with the
332 composition of New Caledonian soils and water associated with weathered ultramafic rocks
333 (Enright et al. 2001). The precipitated iron- and aluminum oxides and aluminosilicate clay
334 minerals formed a fine-grained crust on both internal and external surfaces (Figs 6–8,

335 Supplement), which helped prevent complete collapse of the leaf during burial. The aluminum
336 content prevents the early-formed amorphous oxides from forming larger crystals (Schulze
337 and Schwertmann 1984), promoting the preservation of fine morphological details such as
338 stomata (Fig. 6F, 6G).

339 Aluminum and silicon are depleted by initial microbially-mediated precipitation, and the
340 abundance of iron results in the further precipitation of predominantly iron oxide minerals
341 rather than aluminosilicate clays (Locatelli et al. 2017). Acidic conditions enhanced by decay
342 within the leaf promote the formation of goethite rather than hematite, as evidenced by Raman
343 spectroscopy of leaf tissues (Fig. 4C). The duricrust, in contrast, contains a combination of
344 goethite and hematite, indicating that the sediment pore waters were less acidic (Fig. 4A, 4B),
345 consistent with soil pH measurements from previous studies (Read et al. 2006, table 3).

346 The three-dimensional nature of the fossil leaves (Figs 3A, 6A) and associated, seeds,
347 flowers, and wood fragments indicates that the duricrust formed rapidly, prior to significant
348 decay and collapse. Leaf fossils were not found in the sediments outside the duricrust,
349 indicating that its formation was integral to their preservation. Duricrusts form rapidly when
350 previously waterlogged conditions are followed by dry intervals (Fritsch et al. 2002). The
351 precipitation of dense iron oxide cements reduces the porosity and permeability, which reduces
352 the rate of oxidative destruction of leaf tissues and permits permineralization/petrifaction and
353 replication to occur. Portions of the leaf encased in early aluminosilicate clays and oxides
354 survive as small carbonaceous lenses, but the preservation of anatomy relies very largely on
355 mineralization of morphological features (Fig. 3).

356 The highly oxidizing fluvial and lateritic environments in New Caledonia are not generally
357 conducive to plant preservation. However, duricrusts with root traces are common features of

the New Caledonian fluvio-lacustrine deposits, and although leaf fossils are rare (Folcher et al. 2015), those reported here show the potential of duricrust horizons that formed on ultramafic terrains as a source of exceptionally preserved plant fossils.

ACKNOWLEDGMENTS

We are grateful to the National Geographic Society for funding field work in April, 2013; the Yale Institute of Biospheric Studies and the Yale Peabody Museum of Natural History for funding ERL's research; H. Petermann and Z. Jiang for assistance with Raman spectroscopy and XRD respectively; the Institut de Recherche pour le Développement (IRD) for aid with field work; P.R. Crane for comments on the manuscript, and S.L. Wing and the late L.J. Hickey for helpful discussion. The final version was improved by comments from the editor P.J. Orr and two anonymous reviewers.

REFERENCES

Arana, R., López-Aguayo, F., Velilla, N., and Rodríguez Gallego, M., 1979, Mineralizaciones de hierro en el travertino de Lanjarón (Granada): Acta Geologica Hispanica, v. 14, p. 106–112.

Bourdon E., and Podwojewski P., 1988, Morphopédologie des formations superficielles dans le Sud de la Nouvelle-Calédonie (Rivière des Pirogues, Plaine des Lacs). In: Rapports scientifiques et techniques, Sciences de la Terre. ORSTOM, 43 p.

Chaney, D.S., and DiMichele, W.A., 2007, Paleobotany of the classic redbeds (Clear Fork Group – Early Permian) of north central Texas, in Wong, Th. E., ed,. Proceedings of the XVth

International Congress on Carboniferous and Permian Stratigraphy, 10–16 August 2003, Utrecht, the Netherlands, p. 357–366.

Chaney, D.S., Mamay, S.H., DiMichele, W.A., and Kerp, H., 2009, *Auritifolia* gen. nov., probable seed plant foliage with comioid affinities from the Early Permian of Texas, U.S.A.: International Journal of Plant Sciences, v. 170, p. 247–266.

Chevillotte, V., Chardon, D., Beauvais, A., Maurizot, P., and Colin, F., 2006, Long-term tropical morphogenesis of New Caledonia (Southwest Pacific): Importance of positive epeirogeny and climate change: Geomorphology, v. 81, p. 361–375.

Cluzel, D., Maurizot, P., Collot, J., and Sevin, B., 2012, An outline of the geology of New Caledonia; from Permian-Mesozoic southeast Gondwanaland active margin to Cenozoic obduction and supergene evolution: Episodes, v. 35, p. 72–86.

Cornell, R., 1985, Effect of simple sugars on the alkaline transformation of ferrihydrite into goethite and hematite: Clays and Clay Minerals, v. 33, p. 219–227.

Cornell, R., and Giovanoli, R., 1985, Effect of solution conditions on the proportion and morphology of goethite formed from ferrihydrite: Clays and Clay Minerals, v. 33, p. 424–432.

Cornell, R., Giovanoli, R., and Schindler, P., 1987, Effect of silicate species on the transformation of ferrihydrite into goethite and hematite in alkaline media: Clays and Clay Minerals, v. 35, p. 21–28.

Cornell, R., Giovanoli, R., and Schneider, W., 1989, Review of the hydrolysis of iron (III) and the crystallization of amorphous iron (III) hydroxide hydrate: Journal of Chemical Technology and Biotechnology, v. 46, p. 115–134.

403 Cornell, R.M., and Schwertmann, U., 2006, The iron oxides: structure, properties, reactions,
404 occurrences and uses. John Wiley & Sons.
405 Crane, P.R., and Dilcher, D.L., 1984, *Lesqueria*: an early angiosperm fruiting axis from the mid-
406 Cretaceous: Annals of the Missouri Botanical Garden, v. 71, p. 384–402.
407 Crawford, A., Meffre, S., and Symonds, P., 2003, 120 to 0 Ma tectonic evolution of the
408 southwest Pacific and analogous geological evolution of the 600 to 220 Ma Tasman Fold
409 Belt System: Geological Society of America Special Papers, v. 372, p. 383–403.
410 Cudennec, Y., and Lecerf, A., 2006, The transformation of ferrihydrite into goethite or hematite,
411 revisited: Journal of Solid State Chemistry, v. 179, p. 716–722.
412 Dunn, K.A., McLean, R.J.C., Upchurch, G.R., and Folk, R.L., 1997, Enhancement of leaf
413 fossilization potential by bacterial biofilms: Geology, v. 25, p. 1119–1122.
414 Eissen, J.P., Crawford, A.J., Cotton, J., Meffre, S., Bellon, H., and Delaune, M., 1998,
415 Geochemistry and tectonic significance of basalts in the Poya terrane, New Caledonia:
416 Tectonophysics, v. 284, p. 203–219.
417 Enright, N., Rigg, L., and Jaffré, T., 2001, Environmental controls on species composition along
418 a (maquis) shrubland to forest gradient on ultramafics at Mont Do, New Caledonia: South
419 African Journal of Science, v. 97, p. 573–580.
420 Fandeur, D., Juillot, F., Morin, G., Olivi, L., Cognigni, A., Ambrosi, J.-P., Guyot, F., and Fritsch,
421 E., 2009, Synchrotron-based speciation of chromium in an oxisol from New Caledonia:
422 Importance of secondary Fe-oxyhydroxides: American Mineralogist, v. 94, p. 710–719.
423 Fernández-Remolar, D.C., and Knoll, A.H., 2008, Fossilization potential of iron-bearing minerals
424 in acidic environments of Rio Tinto, Spain: Implications for Mars exploration: Icarus, v. 194,
425 p. 72–85.

426 Folcher, N., Sevin, B., Quesnel, F., Lignier, V., Allenback, M., Maurizot, P., and Cluzel, D.,
427 2015, Neogene terrestrial sediments: a record of the post-obduction history of New
428 Caledonia: Australian Journal of Earth Sciences, v. 62, p. 479–492.
429 Fordham, A., Merry, R.H., and Norrish, K., 1984, Occurrence of microcrystalline goethite in an
430 unusual fibrous form: Geoderma, v. 34, p. 135–148.
431 Fritsch, E., Montes-Lauar, C., Boulet, R., Melfi, A., Balan, E., and Magat, P., 2002, Lateritic and
432 redoximorphic features in a faulted landscape near Manaus, Brazil: European Journal of Soil
433 Science, v. 53, p. 203–217.
434 Gaina, C., Müller, R.D., Royer, J.-Y., Stock, J., Hardebeck, J., and Symonds, P., 1998, The
435 tectonic history of the Tasman Sea: A puzzle with thirteen pieces: Journal of Geophysical
436 Research, v. 103, p. 12413–12433.
437 Garrouste, R., Munzinger, J., Leslie, A., Fisher, J., Folcher, N., Locatelli, E., Foy, W., Chaillon,
438 T., Cantrill, D.J., Maurizot, P., Cluzel, D., Lowry, P.P. II, Crane, P., Bahain, J.-J., Voinchet,
439 P., Jourdan, H., Grandcolas, P., and Nel, A., 2021, New fossil discoveries illustrate the
440 diversity of past terrestrial ecosystems in New Caledonia: Scientific Reports, v. 11, 18388.
441 Guillon J.H., Trescases J.J., Riviere J.L., Saos M.C. and Schmidt M., 1972, Carte géologique à
442 l'échelle du 1/50000. Notice explicative sur la feuille Prony. Bureau de Recherches
443 Géologiques et Minières, Orléans, France.
444 Hanesch, M., 2009, Raman spectroscopy of iron oxides and (oxy) hydroxides at low laser power
445 and possible applications in environmental magnetic studies: Geophysical Journal
446 International, v. 177, p. 941–948.
447 Hayes, D.E., and Ringis, J., 1973, Seafloor spreading in the Tasman Sea: Nature, v. 243, p. 454–
448 458.

449 Herbillon, A.J., and Nahon, D., 1988, Laterites and laterization processes, in Stucki, J.W.,
450 Goodman, B.A., and Schwertmann, U. (eds.) Iron in soils and clay minerals. Reidl,
451 Dordrecht, Holland, p. 779-796.
452 Isnard, S., L'huillier, L., Rigault, F., and Jaffré, T., 2016, How did ultramafic soils shape the
453 flora of the New Caledonian hotspot? Plant Soil, v. 403, p. 53–76.
454 Jaffré, T., 1992, Floristic and ecological diversity of the vegetation on ultramafic rocks in New
455 Caledonia. In Baker, A.J.M., Proctor, J., and Reeves, R.D. (eds) The vegetation of ultramafic
456 (serpentine) soils: Proceedings of the first international conference on serpentine ecology.
457 Intercept, Andover, Hampshire, England, 101–107.
458 Kanellopoulos, C., Thomas, C., Xirokostas, N., and Ariztegui, D., 2019, Banded iron travertines
459 at the Ilia Hot Spring (Greece): an interplay of biotic and abiotic factors leading to a modern
460 banded iron formation analogue? The Depositional Record, v. 5, p. 109–130.
461 Konhauser, K.O., 1998, Diversity of bacterial iron mineralization: Earth-Science Reviews, v.
462 443, p. 91–121.
463 Konhauser, K.O., and Urrutia, M.M., 1999, Bacterial clay authigenesis: A common
464 biogeochemical process: Chemical Geology, v. 161, p. 399–413.
465 Kryshtofovich, A., 1944, The mode of preservation of plant fossils and its bearing on the
466 problem of coal formation: American Journal of Science, v. 242, p. 57–73.
467 Locatelli, E.R., 2013, The exceptional preservation of leaves in iron-rich sediments from
468 Oceania: Geological Society of America Annual Meeting, Abstracts with Programs, v. 45, p.
469 455.
470 Locatelli, E.R., 2014, The exceptional preservation of plant fossils: a review of taphonomic
471 processes and biases in the fossil record. In: M. Laflamme, J.D. Schiffbauer and S.A.F.

Darroch (Editors), Reading and Writing of the Fossil Record: Preservational Pathways to Exceptional Fossilization: Paleontological Society Papers, v. 20, p. 237–258.

Locatelli, E.R., McMahon, S., and Bilger, H., 2017, Biofilms mediate the preservation of leaf adpression fossils by clays: PALAIOS, v. 32, p. 708–724.

Loeppert, R., and Clarke, E., 1984, Reactions of Fe2+ and Fe3+ in calcareous soils: Journal of Plant Nutrition, v. 7, p. 149–163.

Mamay, S.H., 1989, *Evolsonia*, a new genus of Gigantopteridaceae from the Lower Permian Vale Formation, north-central Texas: American Journal of Botany, v. 76, p. 1299–1311.

Martill, D.M., Bechly, G., and Loveridge, R.F., 2007, The Crato fossil beds of Brazil: window into an ancient world. Cambridge University Press.

Maurizot, P., and Campbell, H.J., 2020, Palaeobiogeography of New Caledonia, *in* P. Maurizot, and N. Mortimer (eds.), New Caledonia: Geology, Geodynamic Evolution and Mineral Resources: Geological Society of London Memoir, 51, p. 189–213.

Maurizot, P., and Collot, J., 2009, Explanatory note of the geological map of New Caledonia, scale 1/500,000: Direction de l'Industrie, des Mines et de l'Energie–Service de la Géologie de Nouvelle-Calédonie. Bureau de Recherches Géologiques et Minières, Noumea.

Maurizot, P., and Mortimer, N., eds. 2020, New Caledonia: Geology, Geodynamic Evolution and Mineral Resources: Geological Society of London Memoir, 51.

Maurizot, P., and Vendé-Leclerc, M., 2009, New Caledonia geological map, scale 1/500,000: Direction de l'Industrie, des Mines et de l'Energie–Service de la Géologie de Nouvelle-Calédonie. Bureau de Recherches Géologiques et Minières.

McCurry, M.R., Cantrill, D.J., Smith, P.M., Beattie, R., Dettman, M., Baranov, V., Magee, C., Nguyen, J.M.T., Forster, M.A., Hinde, J., Pogson, R., Wang, H., Marjo, C.E., Vasconcelos,

P., and Frese, M., 2022, A lagerstätte from Australia provides insight into the nature of Miocene mesic ecosystems: Sciences Advances, v. 8, eabm1406.

Mohr, B.A.R., and Friis, E.M., 2000, Early angiosperms from the Lower Cretaceous Crato Formation (Brazil), a preliminary report: International Journal of Plant Sciences, v. 161, p. S155–S167.

Morris, R., and Ramanaidou, E., 2007, Genesis of the channel iron deposits (CID) of the Pilbara region, Western Australia: Australian Journal of Earth Sciences, v. 54, p.733–756.

Nel, A., and Blot, P., 1990, Paléoentomologie de la paléotufière éocène de Sézanne (Marne, France) (Insectes Odonata, Trichoptera, Hemiptera, Diptera): Entomologica Gallica, v. 2, p. 26–31.

Pacton, M., Fiet, N., and Gorin, G.E., 2007, Bacterial activity and preservation of sedimentary organic matter: the role of exopolymeric substances: Geomicrobiology Journal, v. 24, p. 571–581.

Pelletier, B., 2006, Geology of the New Caledonia region and its implications for the study of the New Caledonian biodiversity. In: C.E. Payri and B. Richer de Forges (Editors), Compendium of marine species from New Caledonia,. Documents Scientifiques et Techniques. IRD, Noumea, pp. 19–32.

Ramanaidou, E.R., and Morris, R.C., 2010, A synopsis of the channel iron deposits of the Hamersley Province, Western Australia: Applied Earth Science, v. 119, p. 56–59.

Read, J., Jaffré, T., Ferris, J.M., McCoy, S., and Hope, G.S., 2006, Does soil determine the boundaries of monodominant rain forest with adjacent mixed rain forest and maquis on ultramafic soils in New Caledonia?: Journal of Biogeography, v. 33, p. 1055–1065.

517 Retallack, G., and Dilcher, D., 2012, Core and geophysical logs versus outcrop for interpretation
518 of Cretaceous paleosols in the Dakota Formation of Kansas: Palaeogeography,
519 Palaeoclimatology, Palaeoecology, v. 329, p. 47–63.
520 Sánchez España, J., Santofimia Pastor, E., and López Pamo, E., 2007, Iron terraces in acid mine
521 drainage systems: A discussion about the organic and inorganic factors involved in their
522 formation through observations from the Tintillo acidic river (Riotinto mine, Huelva, Spain):
523 Geosphere, v. 3, p. 133–151.
524 Schopf, J.M., 1975, Modes of fossil preservation: Review of Palaeobotany and Palynology, v.
525 20, p. 27–53.
526 Schulze, D.G., and Schwertmann, U., 1984, The influence of aluminium on iron oxides: X.
527 properties of Al-substituted goethites: Clay minerals, v. 19, p. 521–539.
528 Schwertmann, U., 1988, Some properties of soil and synthetic iron oxides, in Stucki, J.W.,
529 Goodman, B.A., and Schwertmann, U. (eds.) Iron in soils and clay minerals. Reidl,
530 Dordrecht, Holland, p. 203–250.
531 Schwertmann, U., and Latham, M., 1986, Properties of iron oxides in some New Caledonian
532 oxisols: *Geoderma*, v. 39, p. 105–123.
533 Schwertmann, U., Stanjek, H., and Becher, H.-H., 2004, Long term in vitro transformation of 2-
534 line ferrihydrite to goethite/hematite at 4, 10, 15 and 25ºC: Clay Minerals, v. 39, p. 433–438.
535 Sdrolias, M., Müller, R., and Gaina, C., 2003, Tectonic evolution of the southwest Pacific using
536 constraints from backarc basins: Geological Society of America Special Papers, v. 372, p.
537 343–359.
538 Sevin, B., Maurizot, P., Cluzel, D., Tournadour, E., Etienne, S., Folcher, N., Jeanpert, J., Collot,
539 J., Iseppi, M., Meffre, S., and Patriat, M., 2020, Post-obduction evolution of New Caledonia.

in P. Maurizot, and N. Mortimer (eds.), New Caledonia: Geology, Geodynamic Evolution and Mineral Resources: Geological Society of London Memoir, 51, p. 147–188.

Sevin, B., Ricordel-Prognon, C., Quesnel, F., Cluzel, D., Lesimple, S., and Maurizot, P., 2012, First palaeomagnetic dating of ferricrete in New Caledonia: New insight on the morphogenesis and palaeoweathering of 'Grande Terre': Terra Nova, v. 24, p. 77–85.

Smiley, C.J., Gray, J., and Higgins, L.M., 1975, Preservation of Miocene fossils in unoxidized lake deposits, Clarkia, Idaho, with a section on fossil Insecta by W.F. Barr and J.M. Gillespie: Journal of Paleontology, v. 49, p. 833–844.

Spicer, R.A., 1977, The pre-depositional formation of some leaf impressions: Palaeontology, v. 20, p. 907–912.

Spicer, R.A., 1989, The formation and interpretation of plant fossil assemblages: Advances in Botanical Research, v. 16, p. 95–191.

Spicer, R.A., 1991, Plant taphonomic processes. *in* P.A. Allison and D.E.G. Briggs (eds.), Taphonomy: Releasing the data locked in the fossil record. Plenum, New York and London, 71-113.

Tardy, Y., and Roquin, C., 1998, Dérive des continents. Paléoclimats et altérations tropicales. Editions BRGM, Orleans, ix + 473 pp.

Uruski, C., and Wood, R., 1991, A new look at the New Caledonia Basin, an extension of the Taranaki Basin, offshore North Island, New Zealand: Marine and Petroleum Geology, v. 8, p. 379–391.

Yang, K., Whitbourn, L., Mason, P., and Huntington, J., 2013, Mapping the chemical composition of nickel laterites with reflectance spectroscopy at Koniambo, New Caledonia: Economic Geology, v. 108, p. 1285–1299.

FIGURE 1.—Location of the study area in 'Massif du Sud' of New Caledonia with insets showing position of **A**) New Caledonia in relation to Australia and **B**) position of 'Massif du Sud' within New Caledonia. (Modified from Maurizot and Vende-Leclerc 2009 and Folcher et al. 2015).

FIGURE 2.—Selected angiosperm leaf fossils from Neogene fluvio-lacustrine deposits, 'Massif du Sud', New Caledonia. **A-E**) Preservation of venation. A) F-DIM 0170A; B) F-DIM 0171A, cf. Myrtaceae, sp. 1; C) F-DIM 0172A, Ericaceae; D) F-DIM 0173A; E) F-DIM 0172B, cf. Myrtaceae, sp. 2. **F**) with **G**) a detail showing three dimensional and variable preservation of leaf tissues: F-DIM 0170B. **H**) Three-dimensional preservation and a cast of leaf tissues: F-DIM 0172C.

FIGURE 3.— Backscatter scanning electron micrographs and elemental maps of a section through part of a fossil angiosperm leaf from F-DIM 0170. **A**) Backscatter electron micrograph of a thin section through part of a fossil leaf (the dark area is an epoxy-filled void). Outline indicates the location of the image in B. **B**) Backscatter electron micrograph of the edge of the leaf upper surface showing poorly preserved cell outlines and residual dark carbonaceous material scattered in a mineral matrix. **C)** Elemental maps of the area in B.

FIGURE 4.—Raman spectroscopic analyses of fossil leaves. **A**) Spectrum characteristic of four analysed matrix grains, consistent with hematite. **B**) Spectrum characteristic of the other 11

586 matrix grains, consistent with goethite. **C**) Spectrum characteristic of all grains from analysed
587 fossil leaves, also consistent with goethite.
588
589 **FIGURE 5.**—Scanning electron micrographs of mineral textures from F-DIM 0172. **A**) Fine-
590 grained texture characteristic of the matrix. **B**) Coarse goethite bundles characteristic of infill
591 preservation within vascular tissues. Inset shows location within a leaf vein (Fig. 6D). **C**) Fine-
592 grained goethite bundles characteristic of infill preservation of some vascular tissues and other
593 tissue types. Inset shows location within the vascular tissue. **D**) Nanocrystalline to amorphous
594 texture of mold preservation of stomata and epidermal cells. Inset shows location on a stoma
595 guard cell (Fig. 6G).
596
597 **FIGURE 6.**—Scanning electron micrographs of fossil angiosperm leaves (A in backscatter
598 mode from F-DIM 0170 (see Fig. 3). B, D, F, G, I, J from F-DIM 0172; E from F-DIM 0170; H,
599 K, L from F-DIM 0173). **A**) Cross section through part of a three dimensionally preserved leaf
600 showing the difference in intensity between the matrix and fossil resulting from the different iron
601 oxide minerals and trace elements they contain. The black areas are voids. M = mesophyll, Ab =
602 abaxial (lower) surface, Ad = adaxial (upper) surface, V = Midrib vein. **B**) Part of a fossil leaf
603 showing three-dimensional preservation of tissues. M = mesophyll, V = vascular tissues, E =
604 epidermis. **C**) Vascular tissue replaced by iron oxides, resulting in hollow tubes. **D**) Vascular
605 tissue preserved as internal molds. Center of the image lacks clarity of individual cells, while
606 cells on the left of the image are preserved such that individual cells are distinct. **E**) High fidelity
607 replacement of vascular tissues showing loss of cellulosic cell walls and replacement of lignified
608 secondary cell walls by iron oxides. **F**) Fracture through a leaf showing the walls of epidermal

609 cells and stomata replaced with iron oxides. **G**) Details of a single stoma showing replacement of
610 cells walls. **H**) Adaxial epidermis viewed from the inside of a leaf. In some areas, residual cuticle
611 may be preserved (lower arrow). In others, the cuticle is replaced by iron oxides (upper arrow).
612 **I**) Internal mold of epidermal cells infilled with acicular iron oxides. **J**) Poorly preserved remains
613 of mesophyll (center) surrounded by internal molds of vascular tissues. **K**) Leaf gland showing
614 replacement by iron oxides. **L**) Leaf fragment showing multiple glands (top) and vascular tissues
615 preserved as internal molds.
616
617 **FIGURE 7.**—Scanning electron microscope images of fossil angiosperm leaves showing
618 evidence of biofilms (indicated by arrows) from F-DIM 0173. **A**) Diatom. **B**) Thin strands of
619 EPS. **C**) EPS veils. **D**) Biofilm strands.
620
621 **FIGURE 8.**—Modern angiosperm leaves from a stream south of Les Chutes de Madeleine. **A**)
622 Leaves showing differences in completeness, decay, and encrustation. Left to right: *Homalium*
623 *kanaliense* (Salicaceae), *Grevillea gillivrayi* (Proteaceae), *Tristaniopsis glauca* (Myrtaceae). **B**)
624 EDS spectrum of thick mineral crust (point 1 in E) showing an aluminum-bearing iron oxide. **C**)
625 EDS spectrum of minerals in contact with the leaf (point 2 in H), showing an iron-rich
626 aluminosilicate and iron oxide. **D**-**I**) Scanning electron micrographs. **D**) Transverse section of a
627 leaf impregnated by iron oxides; note the coherent leaf cuticle. **E**) Biofilm comprised of diatoms
628 (D), their extracellular polymeric substance (E), and mineral crust (1). **F**) Detail of mineral crust
629 on the abaxial leaf surface; note the coherent leaf cuticle and stomata. **G**) Partially skeletonized
630 leaf showing the resistance of exposed veins preserved iron oxides. **H, I**) Two of the different
631 diatoms found on all the leaves examined.

FIGURE 9.— Backscatter scanning electron micrographs and elemental maps of the transverse section of the leaf illustrated in Figure 8D rotated to horizontal, adaxial surface at the top.

Supplementary figure.—Backscatter scanning electron micrograph and elemental spectra of points within a section through part of the fossil angiosperm leaf from F-DIM 0170 illustrated in Fig. 3. **A**) Backscatter electron micrograph of a thin section through part of the fossil leaf (the dark area is an epoxy-filled void). Outline indicates the location of the image in B. **B**) Backscatter electron micrograph of the edge of the leaf upper surface showing poorly preserved cell outlines and residual dark carbonaceous material scattered in a mineral matrix. Numbers correspond to the location of EDS spectra in C. **C1**) Iron oxide dominated matrix surrounding the leaf. **C2**) Residual carbonaceous material. **C3**) Mixed aluminosilicate, iron oxide associated with residual carbonaceous material. **C4**) Mixed aluminosilicate, iron oxide within the leaf not directly associated with residual carbonaceous material.

Figure 1

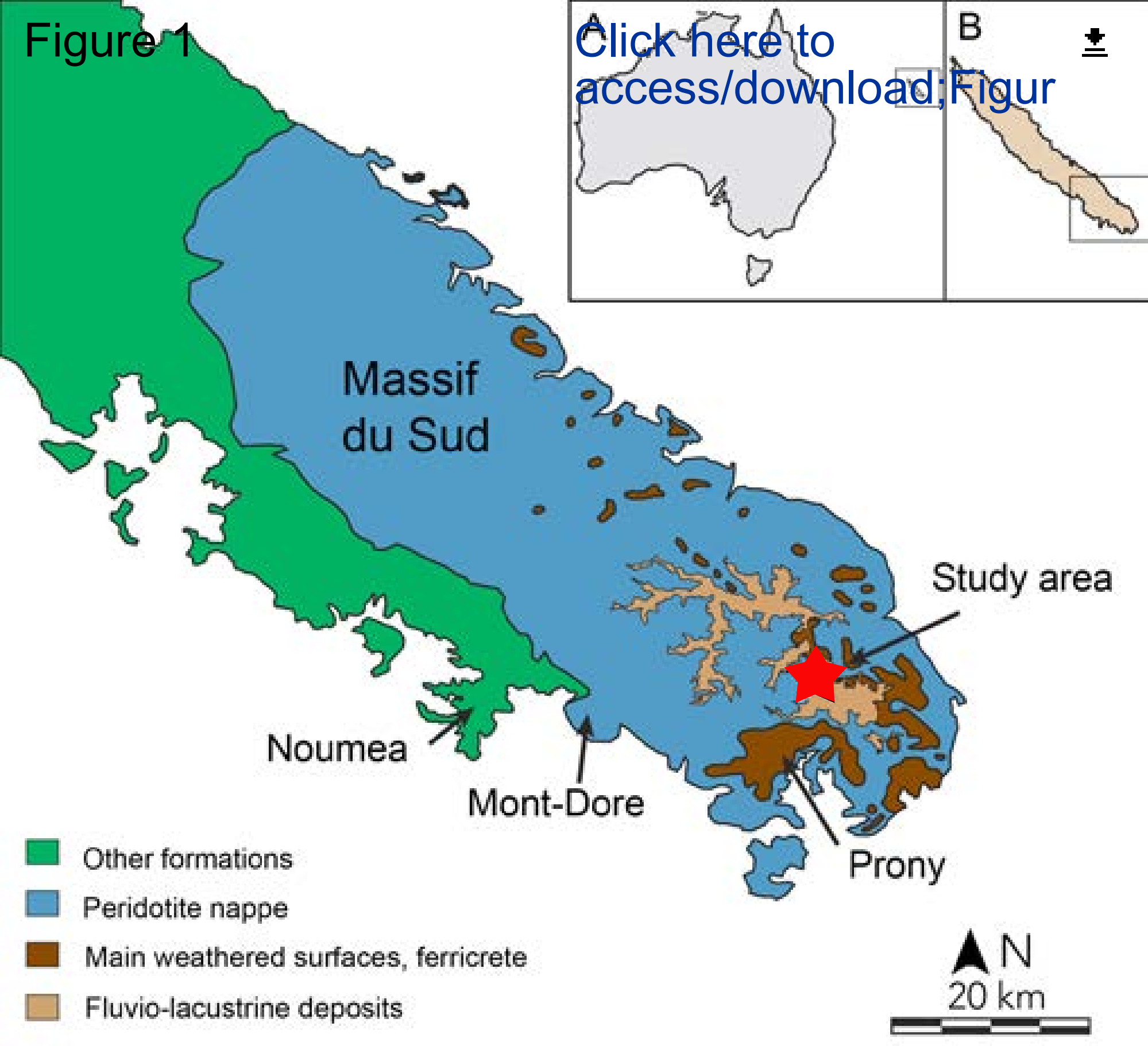
Click here to access/download;Figur
A
B
Massif du Sud
Study area
Noumea
Mont-Dore
Prony
Other formations
Peridotite nappe
Main weathered surfaces, ferricrete
Fluvio-lacustrine deposits
N
20 km

Figure 2

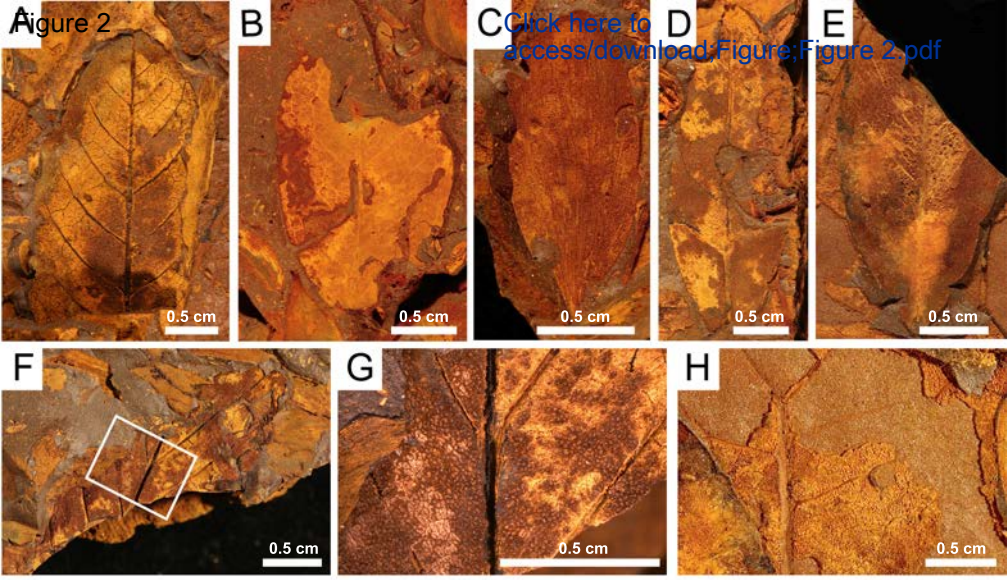

Figure 3

Click here to access/download;Figure;Figure 3.pdf

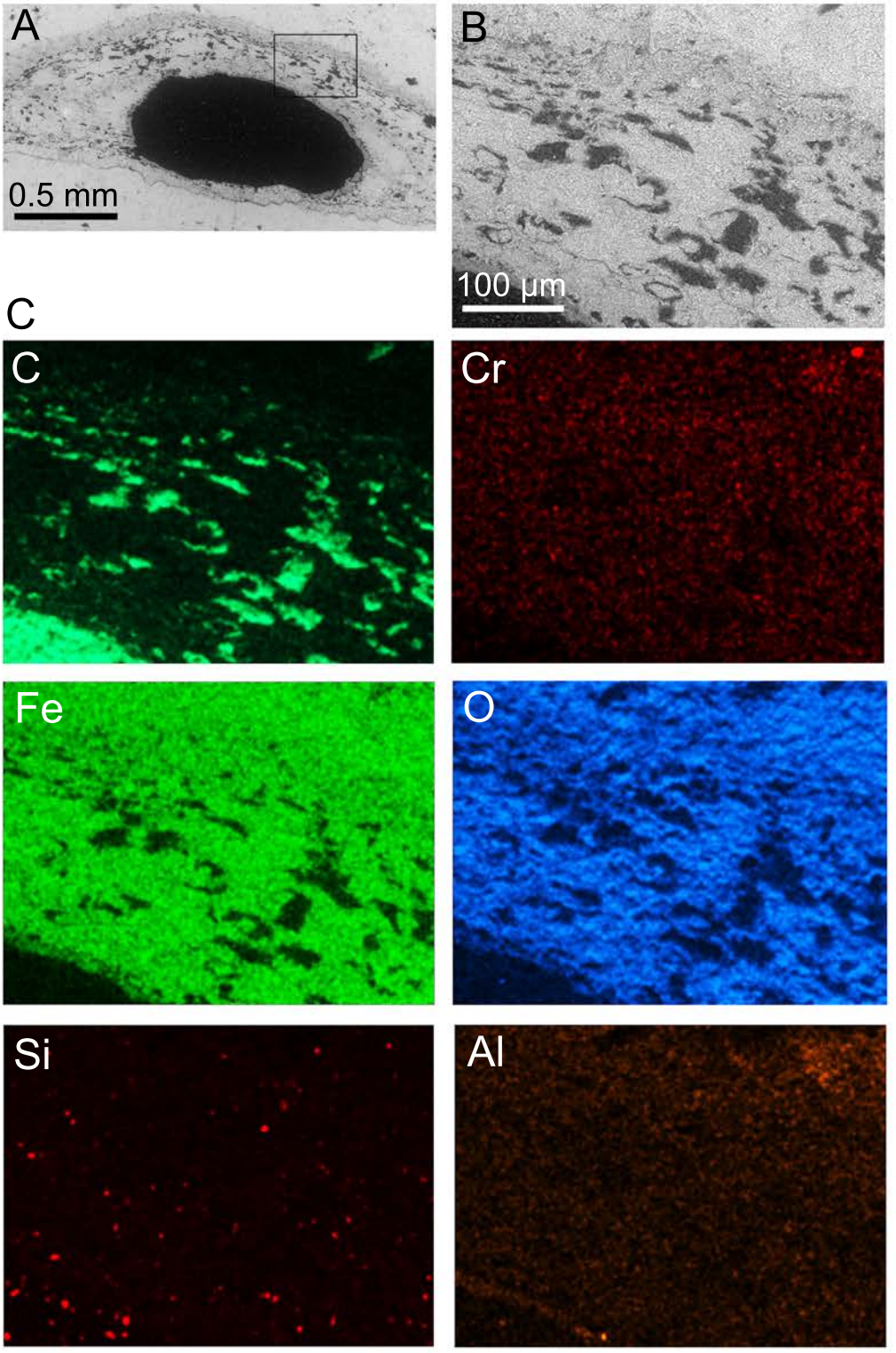

Figure 4

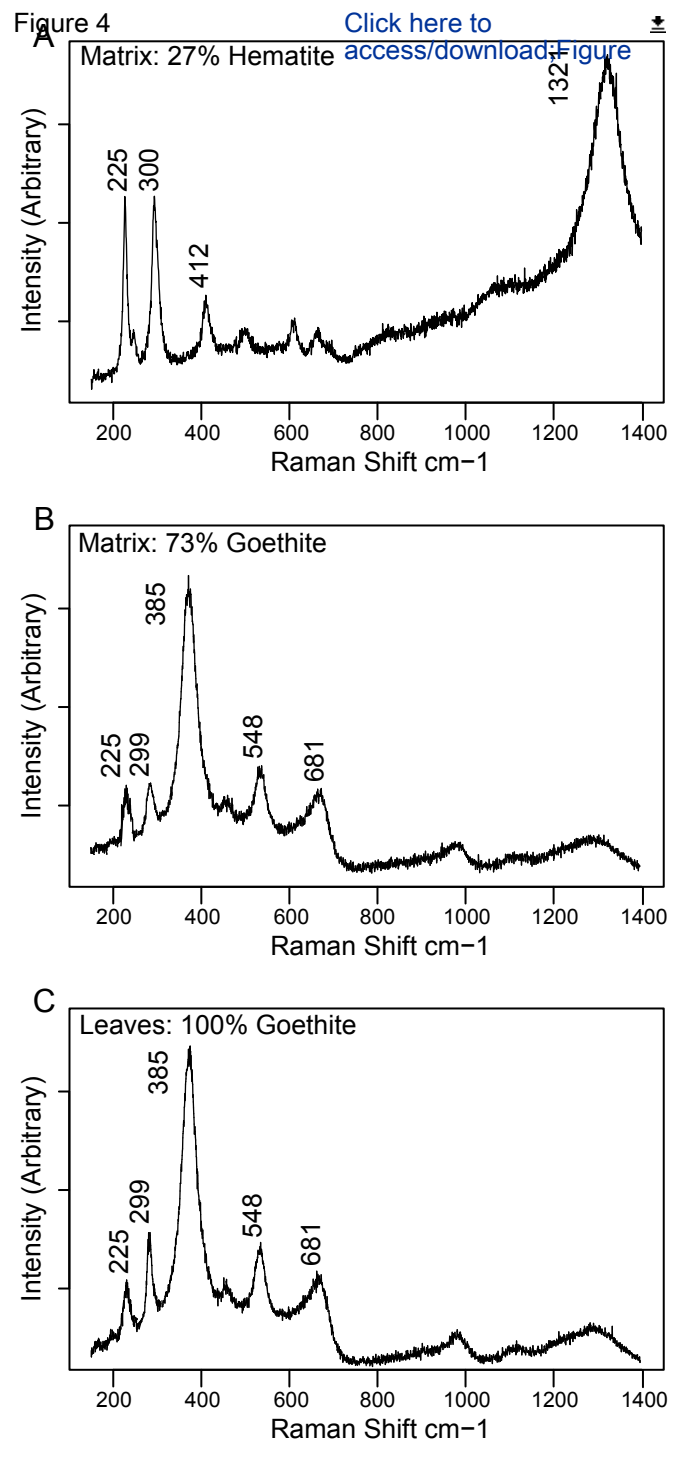

Figure 5

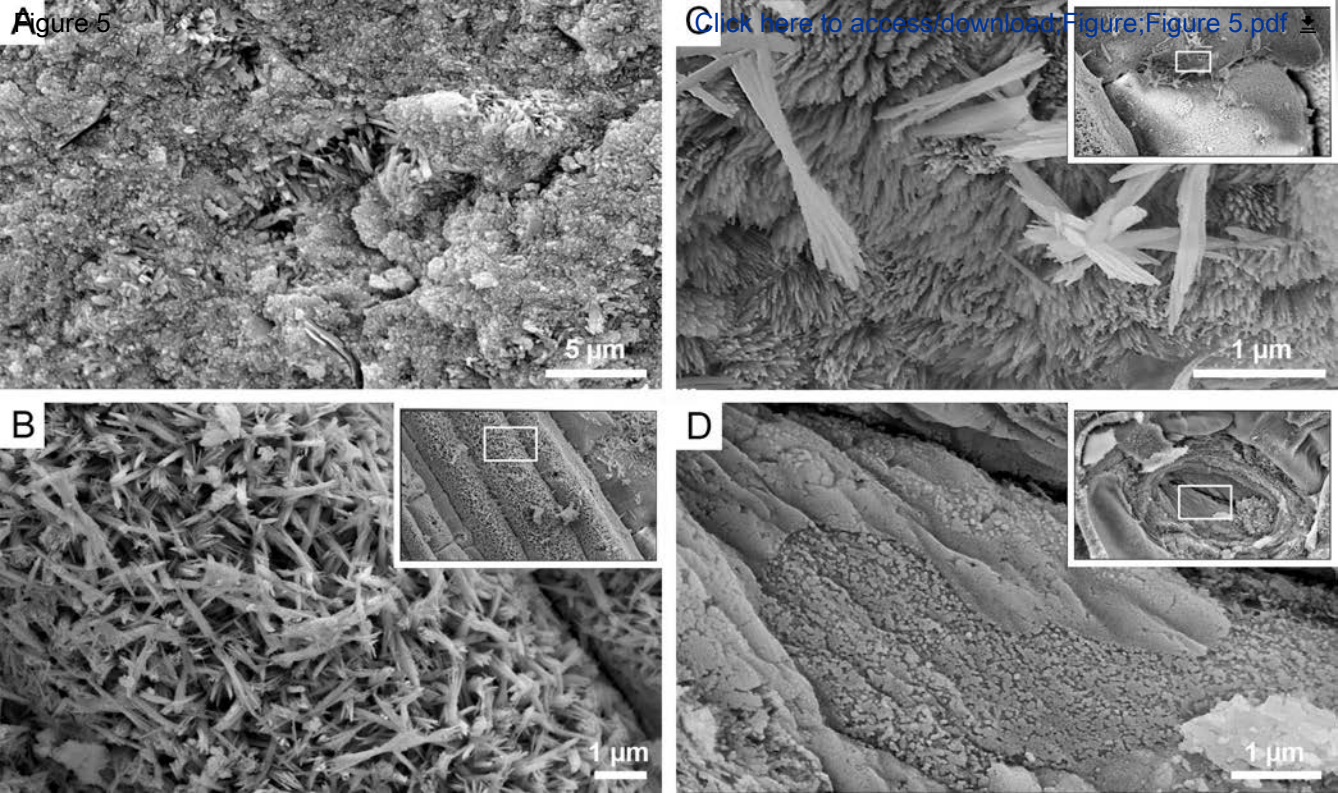

Figure 6

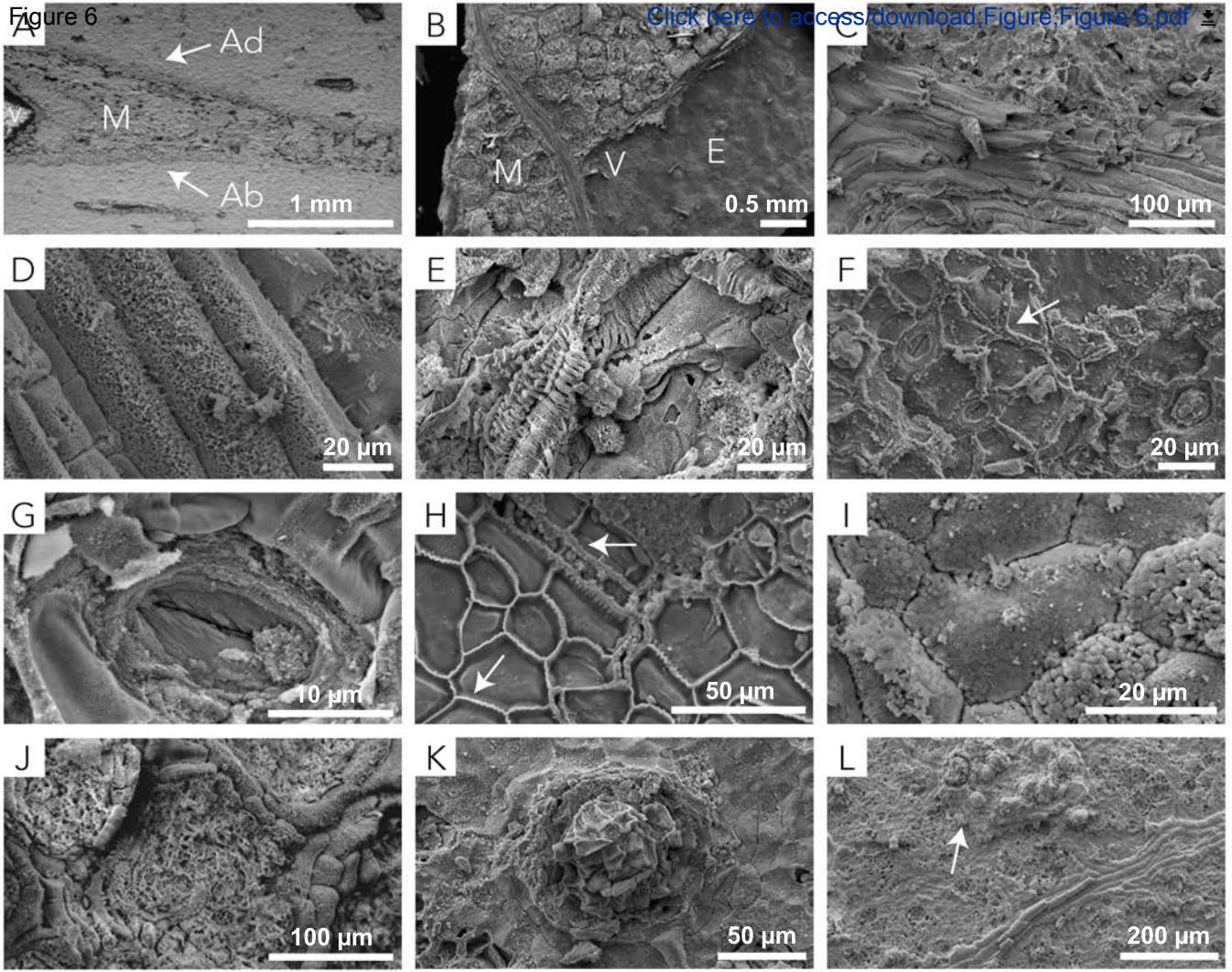

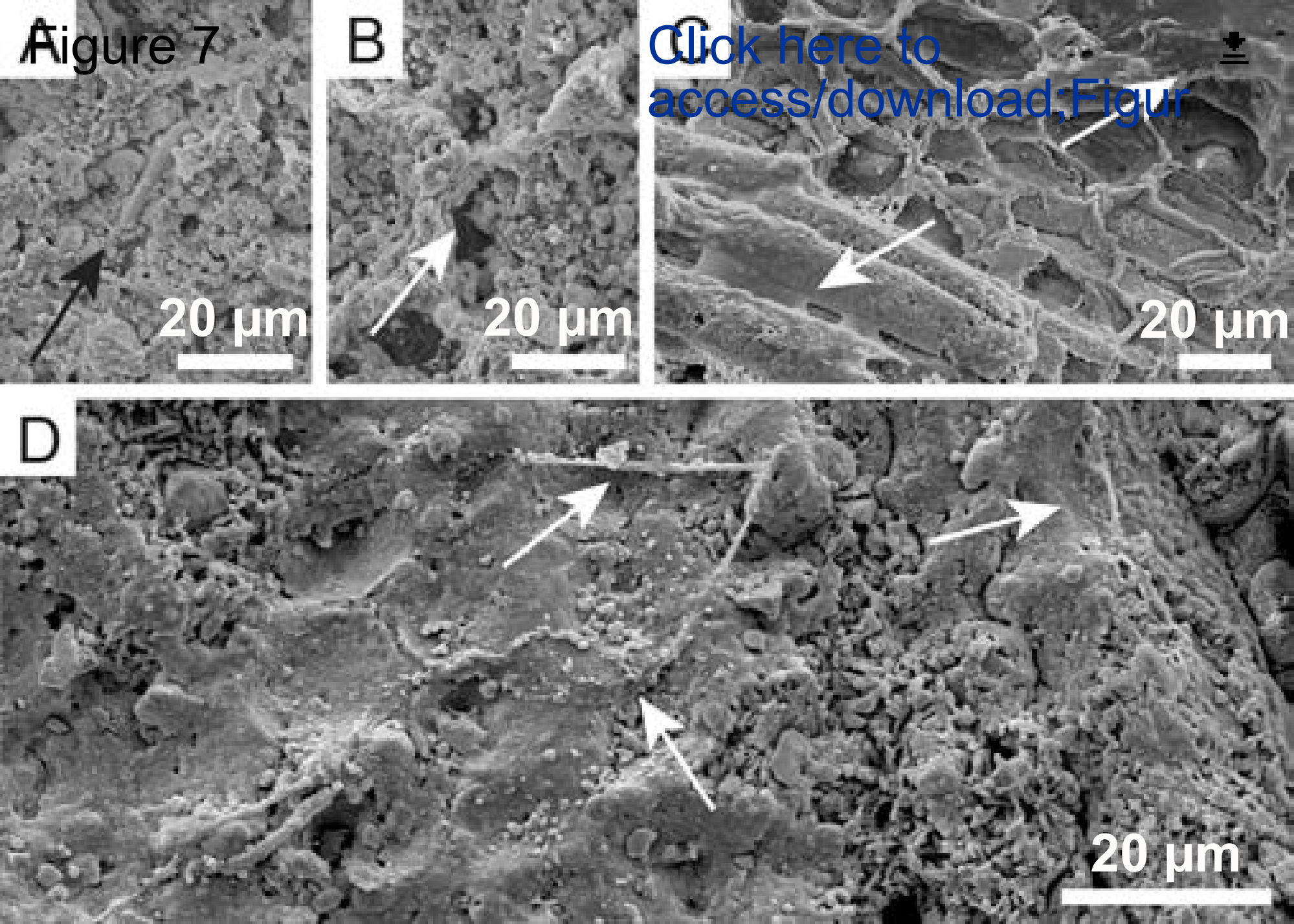
Figure 7
A
B
C
D
20 µm
20 µm
20 µm
20 µm
Click here to access/download;Figur

Figure 8

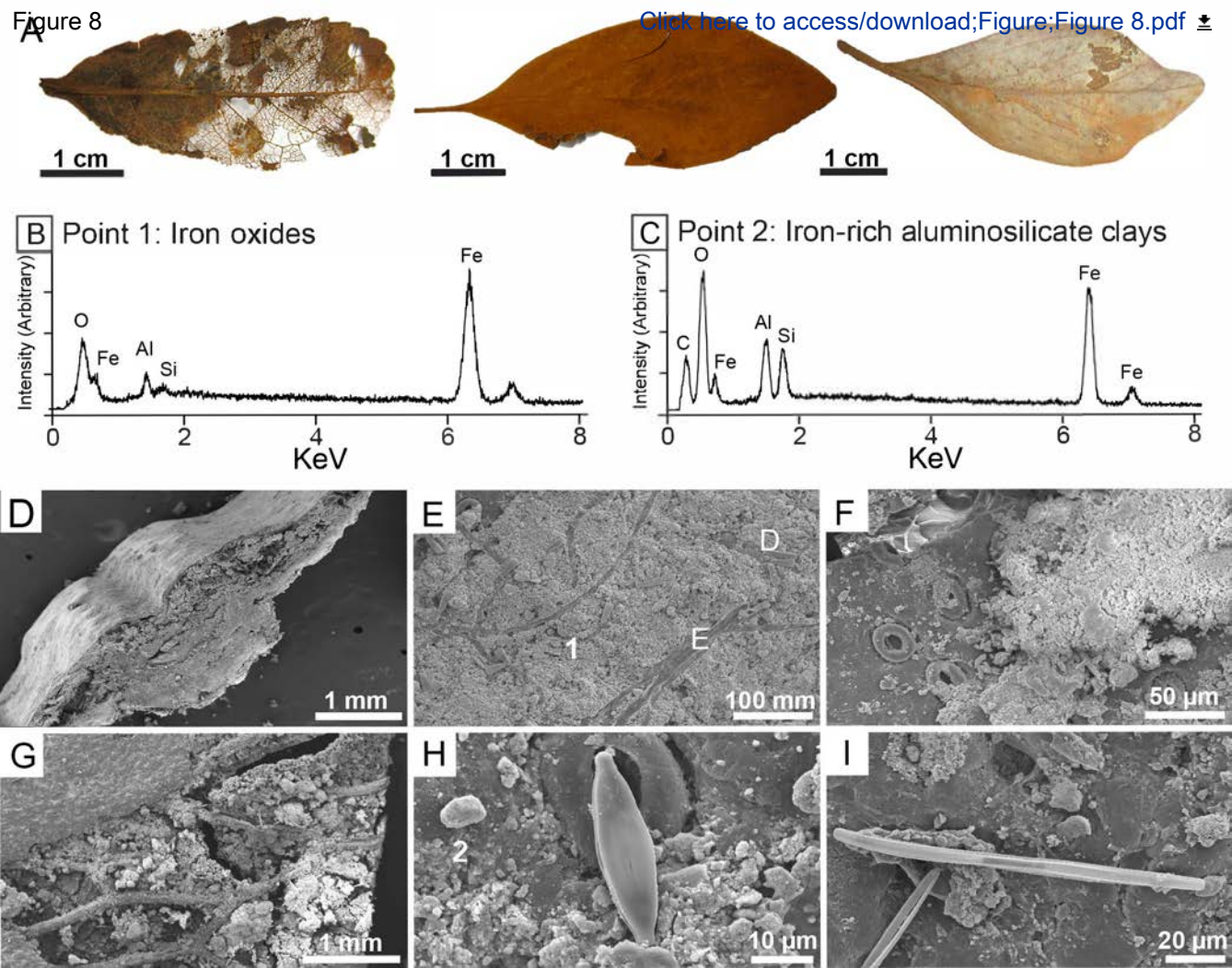

Figure 9

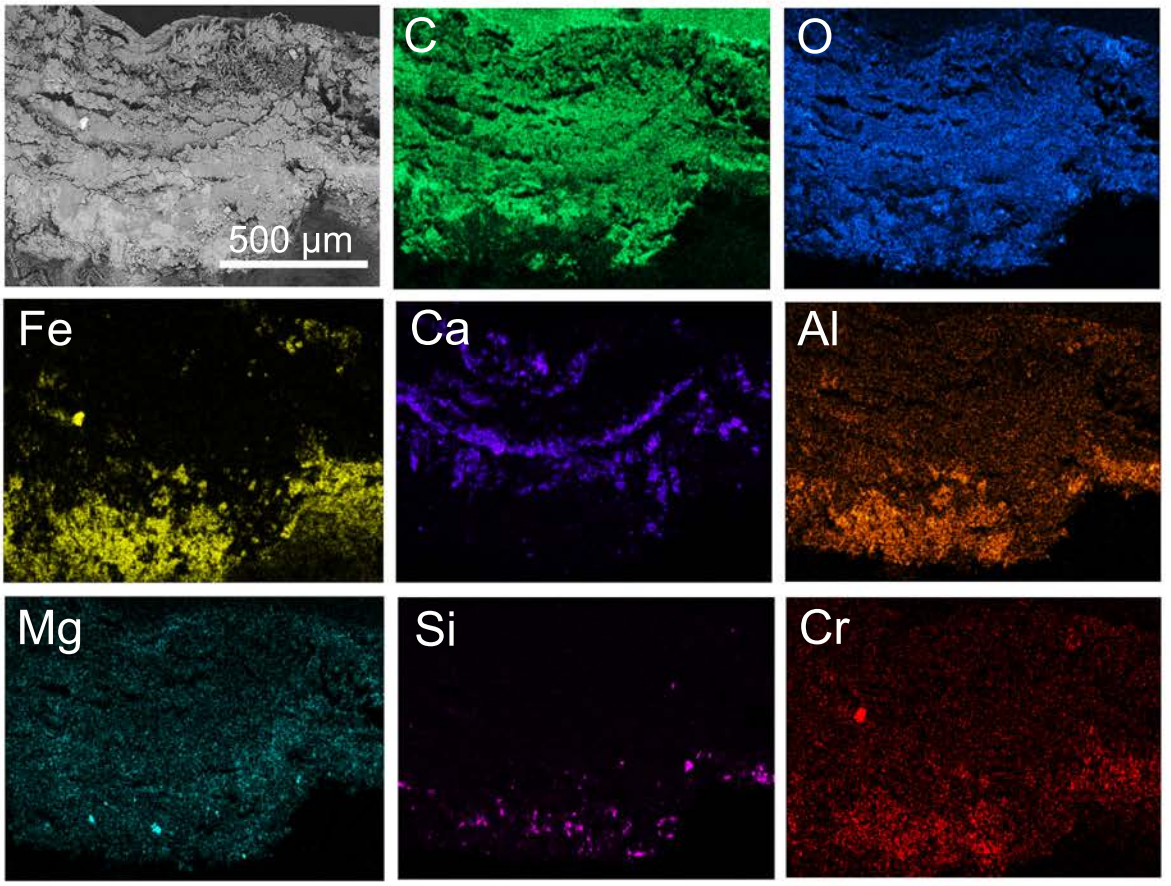

Supplementary Figure